ARTICLE
Journal of Cellular Biochemistry 115:271–280 (2014)

Journal of Cellular Biochemistry

Visualization of Hypoxia-Inducible Factor 1α-p300 Interactions in Live Cells by Fluorescence Resonance Energy Transfer

So Yeon Kim, Myong Jin Lee, Yu-Ran Na, Sang Yoon Kim, and Eun Gyeong Yang*

Center for Theragnosis, Biomedical Research Institute, Korea Institute of Science and Technology, Seoul 136-791, Republic of Korea

ABSTRACT

Hypoxia-inducible factor (HIF)-1α mediates the hypoxia response signaling pathway essential for maintaining cellular homeostasis in low oxygen environments through its complex formation with CBP/p300 in the nucleus. Employing fluorescence resonance energy transfer (FRET), we devised a live-cell interaction assay based on reporter proteins by tagging fluorescent proteins onto the carboxy termini of HIF-1α and p300. The nature of the constructed reporter protein was verified by observing localized distribution, degradation, and stabilization kinetics in cells transfected with the HIF-1α containing plasmid. A mutant HIF-1α incapable of binding to p300 was then utilized to demonstrate insignificant FRET efficiency, thereby confirming that our constructs could effectively probe the direct interaction between HIF-1α and p300. We further examined the effects of small molecules known to modulate the HIF-1α-p300 interaction and transcriptional activity on FRET. Finally, by inhibiting activities of two HIF-specific hydroxylases, HIF-specific prolyl hydroxylase (PHD) 2 and factor inhibiting HIF-1 (FIH-1) with their specific siRNAs, we explored how these HIF-specific hydroxylases contribute to the HIF-1α-p300 interaction by FRET measurements along with HIF-1 mediated transcriptional activation. Therefore, this technique would provide a way to study selective inhibition of either PHD2 or FIH-1 within living cells, and to screen specific inhibitors of HIF-mediated transcription activity for therapeutic applications. J. Cell. Biochem. 115: 271–280, 2014.

KEY WORDS: HIF-1α; p300; FRET; HIF-1α-p300 INTERACTION; TAD; PHD2; FIH-1

The ability of cellular response to low oxygen tension is critical for survival. Oxygen sensing mechanisms mediated by the hypoxia signaling cascade have been extensively studied since the discovery of hypoxia-inducible factor-1 (HIF-1) [Wenger, 2002; Semenza, 2011]. As a transcription factor composed of α and β subunits, HIF-1 up-regulates a broad range of target genes (for a review, see [Semenza, 2003; Brahimi-Horn and Pouyssegur, 2007]), and the stability and activity of HIF-1α are regulated by two oxygen-dependent hydroxylases [Lando et al., 2002; Berra et al., 2003]. These HIF-specific hydroxylases belong to the superfamily of 2-oxoglutarate (2-OG)-dependent non-heme iron dioxygenases, which require oxygen as a co-substrate, providing the molecular basis for their oxygen-sensing function. HIF-specific prolyl hydroxylases (PHDs) control the stability of HIF-1α through post-translational trans-4-hydroxylation of two prolines (Pro402 and Pro564, see Fig. 1A). Hydroxylation of these residues allows for the binding of HIF-1α to the von Hippel–Lindau tumor suppressor protein (VHL) ubiquitin ligase complex, leading to proteosomal degradation [Maxwell et al., 1999; Ohh et al., 2000; Min et al., 2002]. On the other hand, factor inhibiting HIF-1 (FIH-1) has been known to modulate the transcriptional activity, because hydroxylation of HIF-1α at Asn803 (Fig. 1A) prevents the formation of the transcriptional activation complex with CBP/p300 [Ema et al., 1999].

The hydroxylation sites of HIF-1α are localized within two transactivation domains (TADs), N-TAD and C-TAD. While the C-TAD region has been shown to bind to the cysteine/histidine-rich region 1 (CH1) in CBP/p300 [Dames et al., 2002; Freedman et al., 2002; Lando et al., 2002], a recent study has identified that N-TAD interacts with the CH3 domain of CBP/p300 [Ruas et al., 2010]. Once HIF-1α is stabilized by impairment of PHD2 under hypoxia, it is likely that transactivation mediated by N-TAD is constitutively operative, but the C-TAD activity is further regulated

The authors have no conflict of interest.
Grant sponsor: Korean Ministry of Education, Science and Technology; Grant sponsor: KIST.
*Correspondence to: Eun Gyeong Yang, Hwarangno 14-gil 5, Seongbuk-gu, Seoul 136-791, Republic of Korea.
E-mail: eunyang@kist.re.kr
Manuscript Received: 9 january 2013; Manuscript Accepted: 14 August 2013
Accepted manuscript online in Wiley Online Library (wileyonlinelibrary.com): 21 August 2013
DOI 10.1002/jcb.24659 • © 2013 Wiley Periodicals, Inc.

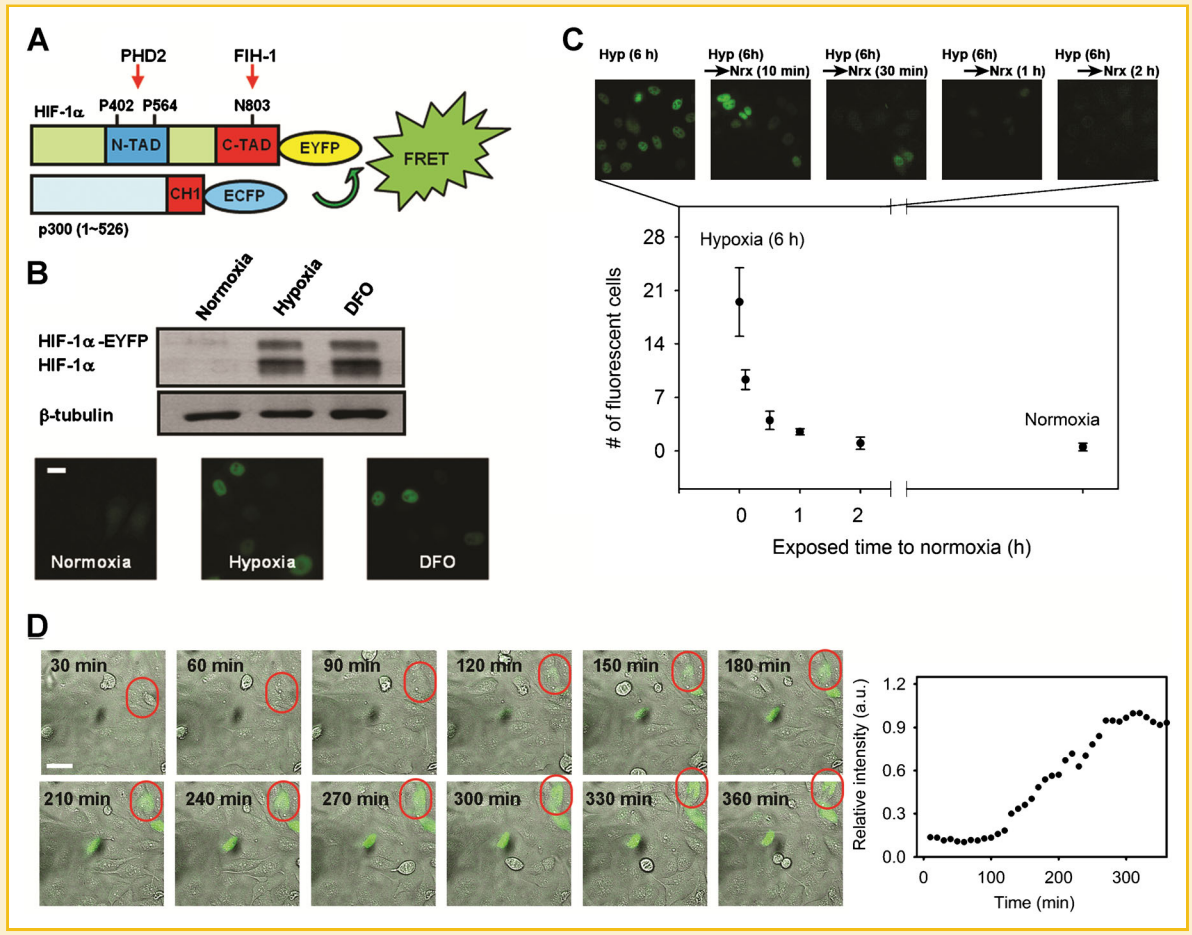

Fig. 1. Design and behavior of HIF-1α–EYFP and p300–ECFP. A: Schematic of HIF-1α tagged with EYFP (HIF-1α–EYFP) and p300 tagged with ECFP (p300–ECFP) constructed for FRET. The positions of fluorescent proteins, two TAD regions, and hydroxylation sites in HIF-1α and the CH1 domain in p300 are indicated. B: Immunoblot and fluorescence microscopic analyses of HeLa cells transfected with the HIF-1α–EYFP plasmid under normoxia or hypoxia. Normoxic cells treated with DFO were also included. Scale bar, 25 μm. C: The degradation kinetics of HIF-1α–EYFP observed in HeLa cells. Transfected HeLa cells were pre-incubated in the hypoxic condition for 6 h, followed by further incubation in the normoxic condition for varying time periods. Cells were then immediately fixed with cold methanol (−20°C) and imaged under a fluorescence microscope. Scale bar, 25 μm. To quantify the kinetics, # of fluorescent cells in a given area was plotted as a function of exposed time to normoxia. Each point represents the mean ± standard error. D: The montage from live cell fluorescence imaging to observe HIF-1α stabilization (see supporting information, Movie S1). HIF-1α–EYFP transfected cells were treated with DFO, and then both fluorescence and white-light images were acquired every 10 min for 14 h. The integrated fluorescence of the cell in a red circle was plotted as a function of incubation time.

by FIH-1. A bifunctional activity of HIF-1α has been demonstrated by revealing two classes of HIF target genes responding differentially to the hypoxic gradient [Dayan et al., 2006]. Considering that PHD2 is easily inactivated by mild oxygen concentrations, and FIH-1 activity maintained even at lower oxygen concentrations [Hirsila et al., 2003; Koivunen et al., 2004; Tian et al., 2011], such oxygen dependence of FIH-1 would confer the ability to make fine discriminations of genes to be induced as a function of oxygen availability [Dayan et al., 2006, 2009; Pelletier et al., 2012].

To understand protein–protein interactions involved in hypoxia, imaging the components of the oxygen sensing mechanisms has been attempted in live cells. Co-localization of CBP and HIF-1α with two different colors was initially employed to elucidate the role of CBP/p300 in regulating HIF-1α mediated transcriptional activation [Ruas et al., 2002, 2005], which was hampered in part by the optical diffraction limit of 200 ∼ 300 nm in the visible region. To observe the interaction of two different proteins at nanometer resolution, fluorescence (Förster) resonance energy transfer (FRET) has been successfully applied by tagging proteins with two different fluorescent proteins, mainly ECFP as a donor and EYFP as an acceptor in living cells (for a review, see [Piston and Kremers, 2007]). FRET measurements enabled the detection of the interactions between HIF-1α and HIF-1β as well as HIF-1α and PHD2 [Wotzlaw et al., 2007, 2010]. Recently, the domain interaction between N-TAD and CH3 was also analyzed based on FRET [Ruas et al., 2010]. Given the non-redundant function roles of C-TAD and N-TAD, the present study was designed to visualize the interaction between C-TAD and CH1 in live cells. Since C-TAD alone would be expected to be stably expressed regardless of oxygen concentrations, we chose the full-length HIF-1α to establish a FRET-based assay for its interaction with p300 containing CH1 using an ECFP/EYFP FRET pair. The role of hydroxylases in HIF-1α-induced transactivation was further investigated by silencing PHD2 and FIH-1, thereby providing the molecular basis for the action of two TADs in HIF-1α.

MATERIALS AND METHODS

CELLS AND REAGENTS

Human HeLa cervical cancer cells and PC3 prostate cancer cells were obtained from the Korea cell line bank and maintained as recommended. Briefly, HeLa cells were cultured in Dulbecco's modified Eagle's medium (Invitrogen) and PC3 cells in RPIM 1640 medium (Invitrogen), supplemented with 10% heat-inactivated fetal bovine serum (Invitrogen), 100 U/ml penicillin G, and 100 μg/ml streptomycin (Invitrogen). Cells were cultured in a humidified incubator containing 5% CO_2 gas at 37°C, and hypoxia was induced by culturing cells in a hypoxic incubator (Model APM-30D, Astec Korea) with 1% O_2, 5% CO_2, 94% N_2 at 37°C. pECFP-N1, pEYFP-N1, pECFP-C1, and pEYFP-C1 from Clontech were used for preparing plasmids containing fluorescent proteins attached to HIF-1α and p300. The HIF-1α full-length coding region was amplified by polymerase chain reaction (PCR) using pcDNA3-HIF-1α as a template with appropriate restriction endonuclease sites attached to the oligonucleotide primers, followed by ligation into pEYFP-N1 or pEYFP-C1. Human p300 (aa 1-528) coding sequences were also similarly introduced into pECFP-N1 or pECFP-C1. The constructed plasmids were designed to produce recombinant HIF-1α and p300 proteins with EYFP and ECFP proteins, respectively, fused at the C- (denoted as HIF-1α-EYFP and p300-ECFP) or N-termini (denoted as EYFP-HIF-1α and ECFP-p300). The triple mutations of L795P, C800R, and L818S in HIF-1α [Gu et al., 2001] were achieved using the Site-Directed Mutagenesis Kit (Muta-Direct™, intron biotechnology). The generated plasmids were verified by sequence analyses. The $p(HRE)_4$-luc plasmid containing four copies of hypoxia responsive element (HRE) [Cho et al., 2005] was used for reporter assays with pSV-β-galactosidase as a normalization control. Anti-HIF-1α and anti-PHD2 were obtained from Cell Signaling and anti-FIH-1 was from Abcam. Anti-β-actin was purchased from Sigma–Aldrich. All other chemicals were of the highest grade of purity commercially available.

TRANSIENT TRANSFECTIONS

DNA transfections were performed using Lipofectamine 2000 (Invitrogen) according to the protocol provided by the manufacture. Briefly, 3×10^4 of HeLa or PC3 cells seeded on fibronectin (25 μg/ml)-coated cover-glass bottom dishes were transfected with appropriate plasmids and incubated overnight. siRNAs for FIH-1 (L-004073-00-0005, On-TARGETPlus SMART POOL) and negative control siRNAs were obtained from Thermo Scientific. siRNA sequences targeting PHD2 regions 885–905 (target sequence, GACGAAAGCCAUGGUUG-CUUG) and 1250–1270 (target sequence, CUUCAGAUUCGGUCG-GUAAAG) [Berra et al., 2003] were synthesized from Eurogene. For siRNA delivery, 2×10^5 of PC3 cells in 6 well plates were transfected twice at 50 nM each with a 24 h interval, and then analyzed next day following the second transfection. For FRET measurements with siRNA treatments, DNAs were co-transfected at the second round of the siRNA transfection, and then 3×10^4 of treated cells were re-plated on fibronectin (25 μg/ml)-coated cover-glass bottom dishes.

CHEMICAL TREATMENTS

For FRET measurements with deferoxamine (DFO) treatment, 150 μM of DFO (final concentration) was added in the media containing 3×10^4 of HeLa cells transfected with p300-ECFP and HIF-1α-EYFP as prepared above and incubated for the appropriate time indicated. For chetomin (CTM) treatment, 3×10^4 of HeLa cells transfected with p300-ECFP and HIF-1α-EYFP as prepared above were incubated in the presence of 600 nM of CTM for 1 h, followed by further addition of DFO (150 μM) for 6 h. To observe the effects of clioquinol (CQ) and metal ion on the formation of the HIF-1α-p300 complex, 3×10^4 of PC3 cells transfected with p300-ECFP and HIF-1α-EYFP were treated with either 15 μM CQ, 50 μM $ZnCl_2$, or both. Cells were observed under a fluorescence microscope after overnight incubation.

FLUORESCENCE IMAGING AND FRET MEASUREMENTS

Nuclear translocation of HIF-1α was observed by imaging HIF-1α-EYFP in HeLa cells under a fluorescence microscope (Deltavision, Applied Precision). For degradation of HIF-1α-EYFP by re-oxygenation, transfected cells under hypoxia for 6 h were transferred into the normal incubator, and fixed with −20°C methanol after the varying incubation periods, followed by fluorescence microscopic examination.

For live cell imaging, we used the Chamlide live cell imaging system (CU 105 with a Chamlide TC chamber, Live Cell Instrument) to control temperature, humidity, and CO_2 gas (37°C, 40% humidity, 5% CO_2). FRET efficiency between p300-ECFP and HIF-1α-EYFP was calculated using ImageJ plugin, FRET analyzer [Hachet-Haas et al., 2006]. Fluorescence images of transfected cells were obtained using a fluorescence microscope (Deltavision, Applied Precision). For ECFP excitation and emission, 436 ± 5 nm and 470 ± 15 nm filters were used, respectively. EYFP fluorescence was visualized with the excitation at 500 ± 10 nm and the fluorescence collection at 535 ± 15 nm. The fluorescence was collected with the same objective for excitation (60X, NA 1.42, PlanApo oil immersion), and imaged on a cooled CCD (Cool SNAP HQ, Photometrics) with a resolution of 512×512 pixels. Briefly, the donor and acceptor bleed through constants denoted as α_D and α_A, respectively, were calculated for cells transfected with the donor p300-ECFP only and the acceptor HIF-1α-EYFP only upon DFO treatment, respectively. More than 10 images for each sample were collected, and data showing good linear regression were selected and averaged. The values for donor and acceptor bleed through constants were ~0.7 and ~0.06, respectively, with the constant exposure time. To obtain FRET efficiency, cells expressing both donor and acceptor fluorescent proteins were selected, and fluorescence intensities including I_{DD} (donor excitation and donor emission), I_{DA} (donor excitation and acceptor emission), and I_{AA} (acceptor excitation and acceptor emission) were collected for each cell. The background was subtracted by using "rolling ball background subtraction" plug-in in the ImageJ program. FRET index was then calculated using the equation, I_{DA}-($\alpha_D I_{DD}$)-($\alpha_A I_{AA}$), where α_D is the donor bleed through, and α_A is the acceptor bleed through. As a negative control, we measured FRET efficiency between free ECFP and EFYP by transfecting cells with empty ECFP and EYFP vectors. FRET index for each cell was measured and the values for the entire nucleus region were integrated and averaged. Two independent experiments were performed.

IMMUNOBLOTTING

For Western blotting, either HeLa or PC3 cells seeded in 6-well plates were transfected with appropriate DNAs and siRNAs as described

above, and whole cell lysates were resuspended in SDS sample buffer, boiled for 5 min and run on SDS-PAGE gels, followed by transfer of the proteins to nitrocellulose membranes. Proteins were then reacted with appropriate antibodies (1:2,000 dilution for anti-HIF-1α, anti-PHD2, and anti-FIH-1) and/or with anti-β-actin antibody (1:5,000 dilution), and visualized by enhanced chemiluminescence (Pierce) with anti-mouse Ig conjugated with horseradish peroxidase as a secondary antibody.

LUCIFERASE REPORTER ASSAY

2×10^5 of PC3 cells in 6 well plates were transfected with 3 μg of $p(HRE)_4$-luc and 0.5 μg of pSV-β-galactosidase (Promega) mixtures. To observe the effect of knock down of hydroxylases on the HIF-1α tansactivation activity, siRNAs were transfected, followed by co-transfection with both siRNAs and reporter DNAs after 24 h. Luminescence was analyzed with a luminometer (Appliskan, Thermo-scientific) using the Bright-Glo Luciferase Assay System (Promega). Measured luciferase activities were normalized to β-galactosidase activities.

QUANTITATIVE REAL TIME-PCR

2×10^5 of PC3 cells in 6 well plates were transfected with appropriate siRNAs twice as described above, and total cellular mRNA from cells was isolated using the RNeasy mini kit (Qiagen) according to the manufacturer's instructions. Aliquots (100 ng) of isolated total RNA were subjected to real time-PCR using TaqMan® RNA-to-Ct™ 1-Step Kit (Applied Biosystems) on StepOne™ (Applied Biosystems). To amplify and quantify the mRNAs of VEGF and β-actin, two sets of primers were used: for VEGF, forward primer (5′-gccttgctgctctacctc-3′) and reverse primer (5′-gcacacaggatggcttg-3′); for β-actin, forward primer (50-acaacggctccggcatgt-30) and reverse primer (5′-cggttggccttggggttc-3′). After a pre-incubation at 46°C for 30 min and an initial melt at 95°C for 10 min, 40 cycles of amplification (95°C for 15 s, 60°C for 60 s) were performed with 5 μM of each primer. The mRNA expression of VEGF was normalized to that of β-actin and compared according to the 2-△△CT method.

RESULTS

SELECTION OF FRET PAIRS

To apply FRET measurements to probe the interaction between HIF-1α and p300, the donor and the acceptor fluorophores attached to the proteins should be placed at a proper distance. Although the crystal structure of the HIF-1α-p300 complex is not yet available, NMR studies have been exploited to elucidate the detailed binding of the HIF-1α C-TAD to the CH1 domain of p300/CBP [Dames et al., 2002; Freedman et al., 2002]. In the complex structures, the distance between the two C-terminal ends was determined to be approximately 2 nm, a little bit shorter than the distance between the two N-terminal ends of ~3 nm. Both values were still much less than the R_0 (~5 nm) value where FRET efficiency for the ECFP-EYFP pair is 50% [Patterson et al., 2000]. However, FRET efficiency employing the full-length HIF-1α (aa 1–826) and the p300 domain (aa 1–528) containing CH1 was unpredictable due to the highly distance-dependent nature of FRET. Accordingly, we prepared p300 and HIF-1α plasmids containing ECFP and EYFP, respectively, at the N- or C-terminal ends, to express proteins attached with the fluorescent proteins at the C-termini (p300-ECFP and HIF-1α-EYFP) or at the N-termini (ECFP-p300 and EYFP-HIF-1α), and mixtures of the two (p300-ECFP and EYFP-HIF-1α; ECFP-p300 and HIF-1α-EYFP) in cells. When we screened cells transfected with such combinations of plasmids for FRET efficiencies, the pair of p300-ECFP and HIF-1α-EYFP as drawn in Figure 1A was found to yield optimal FRET signals (see Fig. 3B for detailed information). These results are in reasonable concordance with the protein sequences that both C-terminal ends are located in close proximity to the C-TAD and CH1 binding domains (Fig. 1A).

CHARACTERIZATION OF HIF-1α AND p300 TAGGED WITH REPORTER PROTEINS

Prior to FRET implementation and exploitation, we first examined the localization and degradation behavior of HIF-1α-EYFP in order to confirm that attachment of the reporter protein EYFP does not affect the function of HIF-1α. HIF-1α is known to be degraded via the ubiquitin-proteosome pathway with a half-life <5 min in normoxia, while oxygen depletion prevents hydroxylation of HIF-1α, thereby leading to its accumulation in the nucleus [Salceda and Caro, 1997; Huang et al., 1998; Kallio et al., 1999]. When HeLa cells transfected with the HIF-1α-EYFP plasmid were analyzed by Western blotting, hypoxic treatment was shown to stabilize both endogenous HIF-1α and exogenously introduced HIF-1α-EYFP which was distinguished by an increased molecular weight of ~27 kDa by EYFP (Fig. 1B). Such stabilization was also seen in the DFO treated cells, whereas normoxic cells exhibited none of the two HIF-1α proteins (Fig. 1B). It should be noted that the amount of the plasmid used for transfection was adjusted not to overexpress exogenous HIF-1α-EYFP. The accumulation of HIF-1α-EYFP in hypoxia was further studied by cellular fluorescence imaging. As shown in Figure 1B, EYFP fluorescence was not observed in normoxic cells, implying that HIF-1α-EYFP could be hydroxylated and degraded similarly as endogenous HIF-1α and free EYFP molecules were not released from HIF-1α-EYFP inside the cell. On the other hand, stable fluorescence of HIF-1α-EYFP was observed to be localized mainly in the nuclei of both hypoxia and DFO treated cells. Similarly to HIF-1α, introducing ECFP to the C-terminal end of p300 did not have any significant effect on its localization behavior. No significant fluorescence from free ECFP was observed in the cell cytoplasm, and strong, localized p300-ECFP fluorescence in the nucleus was dominant (Fig. 2A), in accordance with the previous findings [Girdwood et al., 2003; Cereseto et al., 2005]. In addition, the nuclear localization of p300-ECFP remained unchanged regardless of exposure to DFO (Fig. 3A).

We then proceeded to follow the kinetics of HIF-1α-EYFP degradation by returning hypoxic cells to the normoxic condition. HIF-1α-EYFP transfected cells were exposed to hypoxia for 6 h and then re-oxygenated in the normal condition at 20% oxygen. When cells were instantaneously fixed and examined under a fluorescence microscope, followed by counting the number of fluorescent cells in a given area (~300 μm × 300 μm), nuclear accumulated HIF-1α-EYFP fluorescence evident in hypoxia started to decrease noticeably within 10 min of re-oxygenation, and disappeared almost completely after 30 min of re-oxygenation (Fig. 1C). In contrast to a previous finding

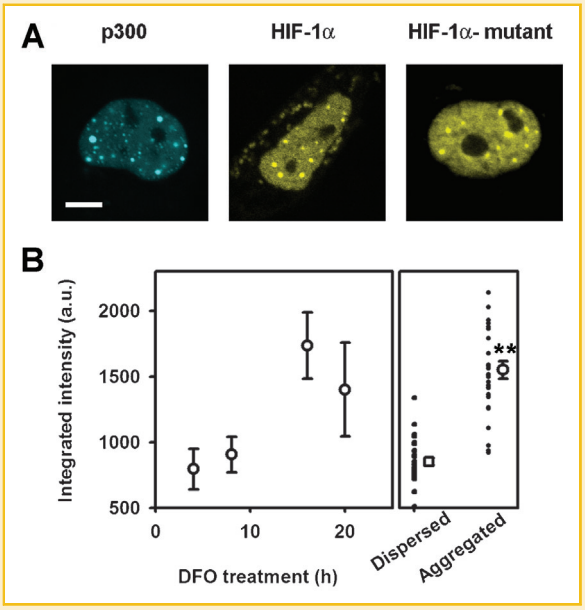

Fig. 2. Effects of DFO treatment on the distribution of HIF-1α-EYFP and p300-ECFP. A: Representative fluorescence images for HeLa cells expressing p300-ECFP, HIF-1α-EYFP, and HIF-1α-EYFP upon DFO treatment for 16 h. Scale bar, 5 μm. B: The left figure shows average fluorescence intensity integrated in the nucleus of HeLa cells (67 different cells) expressing HIF-1α-EYFP as a function of DFO incubation time. Each point represents the mean ± standard error. The cells were also classified into two groups (dispersed and aggregated), and average values of each group were plotted in the right figure ($^{**}P < 0.01$).

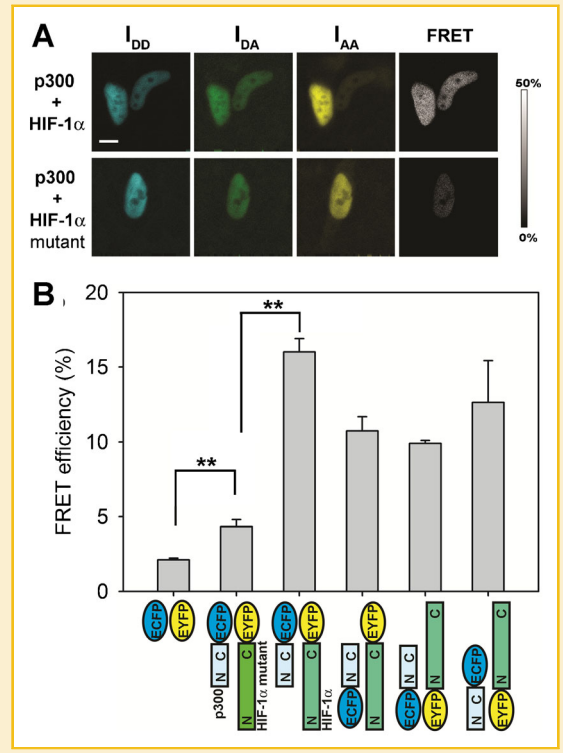

Fig. 3. Measurements of FRET between HIF-1α-EYFP and p300-ECFP. A: Representative fluorescence images of HeLa cells transfected with p300-ECFP/HIF-1α-EYFP and p300-ECFP/HIF-1α-mutant-EYFP, and incubated in the presence of DFO for 6 h. The fluorescence images of the donor (I_{DD}, donor excitation and donor emission) and the acceptor (I_{AA}, acceptor excitation and acceptor emission), FRET without correction (I_{DA}, donor excitation and acceptor emission), and FRET with correction are presented. Scale bar, 5 μm. B: Averaged FRET efficiency with four different constructs described in the text. As negative controls, FRET values between free ECFP/EYFP and p300-ECFP/HIF-1α-mutant-EYFP were measured. Each bar represents the mean ± standard error ($^{**}P < 0.01$).

on the leakage of HIF-1α fluorescence into the cytoplasm at the early stage of re-oxygenation ascribed to the export to the cytoplasm followed by degradation of HIF-1α [Groulx and Lee, 2002], cellular fluorescence at 10 min of re-oxygenation in our study was mostly localized in the nucleus but rarely detected in the cytoplasm. In addition to the degradation kinetics, we further observed the kinetics of HIF-1α-EYFP stabilization after treating cells with DFO (Fig. 1D). Live cell time-lapse imaging with HIF-1α-EYFP for 14 h clearly illustrated the accumulation of HIF-1α, and the integrated fluorescence intensity reached the maximum at ~5 h of DFO treatment. The fluorescence from HIF-1α-EYFP then decreased due to the photobleaching of EYFP (see supporting information, Movie S1), consistent to the photobleaching rate from free EYFP (data not shown).

Next, we closely examined the distribution of nuclear fluorescence from HIF-1α-EYFP. Upon treatment of HeLa cells with DFO for 6 h, HIF-1α-EYFP was relatively evenly distributed in the nucleus (Fig. 1B,C). In contrast, bright, spherical-shaped structures were observed in the cells exposed to DFO for 16 h (Fig. 2A), in agreement with the previous reports [Ruas et al., 2002, 2005; Wotzlaw et al., 2010]. The average fluorescence intensity integrated in the nucleus of HeLa cells expressing HIF-1α-EYFP was proportional to DFO incubation time, and when we classified cells into two groups of dispersed and aggregated, the average value of aggregated was higher than the dispersed (Fig. 2B). On the other hand, we confirmed that the fluorescence intensity of cellular EYFP itself does not change significantly upon treating HeLa cells with DFO for 6 h (see supporting information, Fig. S1). Therefore, it is likely that these bright punctuated fluorescent structures suggesting high aggregation and accumulation of HIF-1α-EYFP develop more prominently with time of DFO incubation, although not all of the cells had such aggregated structures. Intriguingly, cells expressing HIF-1α-mutant-EYFP incapable of binding to p300 also showed these speckle-like structures (Fig. 2A), implying that these structures might not reflect the binding of HIF-1α to p300. In addition, cells expressing p300-ECFP exhibited speckle-like structures even in the absence of DFO similarly as those expressing HIF-1α-EYFP (Fig. 2A).

FRET ANALYSIS FOR THE HIF-1α-p300 INTERACTION

After demonstrating that HIF-1α tagged with a fluorescent protein retained its hypoxia-responsive behavior, we began an exploration of cellular FRET measurements for probing the interaction between HIF-1α and p300. Since the fluorescence intensity from EYFP remained unchanged upon DFO treatment for 6 h (data not shown), we assumed that FRET efficiency would not be affected by use of a hypoxia mimic

reagent DFO. We first used HeLa cells expressing free ECFP and EYFP as a negative control to confirm that FRET between these two fluorescent proteins is almost negligible (~2%) in our experimental condition (Fig. 3B). To validate that the observed cellular FRET signal is originated from the protein–protein interaction rather than accidental proximate localization of the two fluorophores, we generated a HIF-1α triple mutant in which Leu795, Cys800, and Leu818 of the HIF-1α C-TAD were replaced to Pro, Arg, and Ser residues, respectively [Gu et al., 2001]. It was previously shown that the single mutants, L795P, C800R, and L818S are impaired in their binding ability to p300, thereby abolishing hypoxia-induced transcriptional activity [Gu et al., 2001]. Fluorescence images from the donor p300-ECFP, the acceptor HIF-1α-EYFP and FRET were obtained for HeLa cells co-expressing p300-ECFP and HIF-1α-EYFP (Fig. 3A). When compared with the cells transfected with the wild-type HIF-1α-EYFP, FRET efficiency was dramatically reduced in the HeLa cells transfected with the HIF-1α-mutant-EYFP (Fig. 3A). The averaged FRET efficiency for the wild type HIF-1α sample was ~16%, showing the largest among samples with varying combinations of plasmids (Fig. 3B). Although the mutant HIF-1α sample had a four times smaller FRET efficiency (~4%, Fig. 3B), this slightly larger value than that for the ECFP/EYFP negative control could be originated from the transient interaction between two proteins [Hager et al., 2009] since the diffusive motion of a transcription factor is relatively slow [Carrero et al., 2003; Mueller et al., 2010]. Other possibilities, however, such as homo energy transfer, self quenching due to the overexpression of fluorescent proteins, and orientation factor might not be excluded. We further examined FRET efficiency as functions of DFO incubation time and the acceptor/donor ratio, and found no significant changes in our experimental conditions (see supporting information, Fig. S2), implying that most of our data were likely obtained at excessive amounts of acceptors. In any rate, these results suggested that FRET efficiency analyses with p300-ECFP and HIF-1α-EYFP would likely serve as a measure for endogenous HIF-1α-p300 interactions.

EFFECTS OF METAL BINDING MOLECULES ON THE HIF-1α–p300 INTERACTION

Employing the established FRET analysis method, we investigated the effects of small metal binding molecules that are known to modulate the interaction of HIF-1α with p300. We used CTM which has been shown to prevent p300 binding to the HIF-1α C-TAD by ejecting Zn^{2+} from the CH1 domain of p300, leading to attenuation of HIF-1α mediated transcription [Kung et al., 2004; Cook et al., 2009]. When HeLa cells treated with CTM were incubated in the presence of DFO for HIF-1α stabilization, the relative FRET efficiency was significantly reduced to <40% of the control sample (Fig. 4A). We also examined how CQ, a reagent previously shown to activate HIF-1α mediated transcription as a Zn^{2+} chelator [Choi et al., 2006], affects cellular FRET. PC3 cells were chosen for this experiment because they express endogenous HIF-1α even under normoxia, and thus a hypoxia-mimic reagent like DFO is not required for assessing the HIF-1α-p300 interaction (see supporting information Fig. S3). In general, the fluorescence distributions of p300-ECFP and HIF-1α-EYFP proteins in PC3 cells were similar to those in HeLa cells, except for the very bright, aggregated spots observed in the DFO treated HeLa cells. The

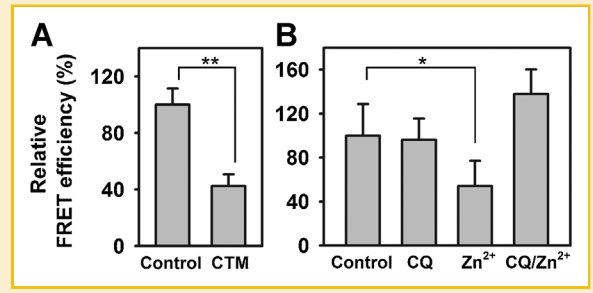

Fig. 4. Effects of small molecules on the FRET efficiency. A: Relative FRET efficiency for HeLa cells treated with or without CTM in the presence of DFO. B: Relative FRET efficiency for PC3 cells in the absence or presence of CQ, Zn^{2+}, and CQ/Zn^{2+}. Each bar represents the mean ± standard error ($^{*}P < 0.05$ and $^{**}P < 0.01$).

average FRET efficiency in PC3 cells was little bit lower (about 12%) than that of HeLa cells. In some cells, HIF-1α-EYFP fluorescence was distributed in the entire region including the cytoplasm, although cytoplasmic fluorescence was rather weaker than nuclear fluorescence. This cytoplasmic fluorescence likely arose from actively expressed HIF-1α-EYFP in normoxic PC3 cells. When PC3 cells were treated with CQ, we observed a mild increase in FRET efficiency regardless of the Zn^{2+} ion presence (Fig. 4B). In contrast, Zn^{2+} itself inhibited the interaction between p300 and HIF-1α consistent to a previous report [Nardinocchi et al., 2010], resulting in decreased FRET efficiency to ~50% of the control (Fig. 4B).

EFFECTS OF SILENCING HYDROXYLASES ON THE HIF-1α–p300 INTERACTION

It has been elucidated that PHD2 is mainly responsible for the hydroxylation of HIF-1α, and thus silencing of PHD2 by siRNA induces accumulation of HIF-1α [Berra et al., 2003], resulting in the N-TAD mediated transactivation. Further silencing of FIH-1 along with PHD2 showed a synergistic effect on the transactivation activity of HIF-1α in normoxic HeLa cells [Dayan et al., 2006]. Therefore, direct comparison of the effects of silencing PHD2 and PHD2/FIH-1 would provide a way to evaluate the relative roles of N-TAD and C-TAD. In this regard, our constructs are beneficial for probing the specific interaction of the HIF-1α C-TAD with the CH1 domain in p300 because of the reporter locations at the C-terminal ends and the absence of CH3 responsible for the N-TAD transactivation. To explore how hydroxylase activities modulate the HIF-1α-p300 interaction and subsequent transcriptional activation, we measured FRET efficiencies by silencing either or both of PHD2 and FIH-1 in PC3 cells. In parallel, the HRE activity, and the expression levels of endogenous HIF-1α and VEGF were also analyzed without transfection of reporter proteins to evaluate gene silencing effects exerted by siRNAs. DFO was also included for comparison since its Fe^{2+} chelating ability has been suggested to inhibit hydroxylases [Hirsila et al., 2005]. Although DFO significantly stabilized HIF-1α (Fig. 5B) with moderately increased FRET efficiency (Fig. 5A), neither the HRE-driven luciferase activity nor the VEGF expression increased proportionally to the amount of HIF-1α (Fig. 5A). Notably, relative

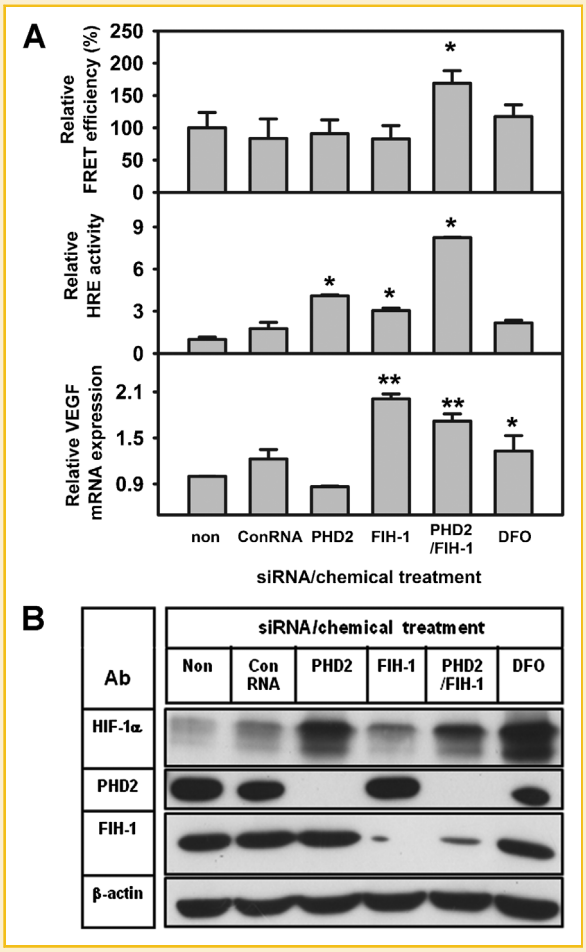

Fig. 5. Effects of silencing hydroxylases using siRNA on HIF-1α signaling pathway. A: Relative FRET efficiency, HRE activity, and VEGF mRNA expression were measured for PC3 cells in the absence or presence of siRNAs for silencing PHD2, FIH-1 or both hydroxylases. As a reference, cells treated with non-coding siRNAs and DFO were also analyzed. Each bar represents the mean ± standard error. B: Immunoblot analyses for HIF-1α, PHD2, and FIH-1 protein levels in samples shown in (A) ($^{*}P < 0.05$ and $^{**}P < 0.01$).

FRET efficiency for the PC3 cells treated with siRNAs against PHD2 and FIH-1 was enhanced by 1.7-fold, while negligible increase was observed in cells treated only with siRNAs against PHD2, as well as with siRNAs against FIH-1 (Fig. 5A). Along with the increased FRET efficiency, cells with silenced PHD2 and FIH-1 had elevated HRE activity and VEGF expression (Fig. 5A), which could be easily explained that stabilized HIF-1α (Fig. 5B) by impaired PHD2 is functional owing to the non-hydroxylated Asn in the C-TAD and its facilitated binding to CH1 of p300. In the case of silencing PHD2 alone, HIF-1α was stably expressed (Fig. 5B), but the interaction between C-TAD and CH1 was hindered by the action of the active FIH-1, resulting in an insignificant FRET increase (Fig. 5A). On the other hand, the enhanced HRE activity was observed (Fig. 5A), implying involvement of the interaction between N-TAD and CH3 facilitated by PHD2 inhibition, whereas VEGF expression was not induced (Fig. 5A). When only FIH-1 was suppressed, HIF-1α was not accumulated through the action of active PHD2 (Fig. 5B), which resulted in no change in FRET efficiency (Fig. 5A). Surprisingly, FIH-1 suppression gave rise to a substantial increase in the HRE-driven luciferase activity, and substantially enhanced the VEGF expression level (Fig. 5A), presumably caused by the interaction between C-TAD and CH1. These results showing that the VEGF expression level was not affected by PHD2 silencing but by FIH-1 silencing were in good agreement with a previous study with HeLa cells [Dayan et al., 2006].

DISCUSSION

The assembly of proteins into defined complexes controls a majority of cellular processes. As temporarily in contact with their binding partners, transiently interacting proteins typically require some conditions that promote the interaction such as post-translational modifications and localization to discrete subcellular regions. While in vitro biophysical or biochemical methods provide the most straightforward approach to study these protein–protein interactions, direct access to such interactions in their cellular environment would be essential for revelation of their physiological roles. Accordingly, we constructed reporter proteins to probe the interaction between HIF-1α and p300 in the cellular context. In addition to maintaining native protein characteristics, these reporter proteins displayed the HIF-1α-p300 interaction-dependent FRET efficiency, and responded to small molecule modulators. Furthermore, combination of the FRET assay with transactivation assays allowed us to evaluate the contribution of HIF-specific hydroxylases towards HIF-1α-mediated interactions and transactivation, demonstrating the potential utility of our assay for screening selective inhibitors for the HIF-1 pathway.

When employing exogenously introduced proteins to explore their interactions, it is critically important to confirm that they exhibit normal behaviors. In previous studies to visualize nuclear translocation of HIF-1α by fluorophore-tagged protein construction, it was first described that GFP fused HIF-1α at the N-terminus was neither degraded nor up-regulated under hypoxia in COS7 cells [Kallio et al., 1998]. Another result with ECFP-HIF-1α in HEK293 cells also suggested that reporter tagged proteins were not destructed by proteasome [Ruas et al., 2002; Xie et al., 2005]. On the other hand, recent studies showed that HIF-1α tagged with ECFP was further accumulated under low oxygen conditions in U2O2 cells regardless of the ECFP tagging position [Wotzlaw et al., 2007, 2010]. We also observed that the expression level of HIF-1α-EYFP was effectively modulated by changing the oxygen concentration (Fig. 1). These controversial results could be attributed to the possibility that the fluorescence signal is from free, dissociated fluorescent protein molecules (either GFP or ECFP) from HIF-1α, rather than firmly attached to HIF-1α. Such free fluorescent protein molecules could cause false localization signs presumably owing to their resistance to proteases [Chiang et al., 2001]. Another possibility is that the expression levels of either HIF-1α or related proteins involved in its stability such as PHD2, FIH-1, and VHL might be dependent on the cell types (COS7 and HEK293 vs. HeLa cells). For example, protein

levels of both HIF and PHDs were found to vary in human cancers [Chan et al., 2009], and cell-specific induction of PHD isoforms was shown to be directly correlated with the relative abundance of the PHDs and their relative contribution to the regulation of HIF [Appelhoff et al., 2004].

Although the distribution of p300 has been reported to be dynamically associated with subnuclear domains [Girdwood et al., 2003], appearance of the highly aggregated HIF-1α-EYFP and p300-CFP observed in HeLa cells (Fig. 2) might be unusual. In particular, our results showed that accumulation of highly aggregated fluorescent HIF-1α spots as a function of DFO incubation time (Fig. 2B). Moreover, p300-ECFP started to aggregate after 20 h of transfection even in the absence of DFO (Fig. 2). For distribution analysis of nuclear proteins tagged with fluorescent proteins, it has been recommended that transiently transfected cells be typically examined within 18–24 h post transfection [Carrero et al., 2003], because some over-expressed proteins do not behave as endogenous proteins and exhibit either diffusive distribution or formation of large spherical aggregates. Interestingly, other studies observing such highly aggregated spots were performed by obtaining fluorescence cell images after 36–48 h of transfection [Ruas et al., 2002, 2005, 2010; Wotzlaw et al., 2007, 2010], while we detected those within 24 h. In contrast to these observations, immunofluorescence images of endogenous HIF-1α demonstrated homogenous distribution without such highly aggregated spots [Kallio et al., 1998; Berra et al., 2003; Moroz et al., 2009], suggesting that the highly aggregated spots could be artificial. Unlike HeLa cells, our studies with PC3 cells showed insignificant aggregated HIF-1α and p300 (data not shown). Nonetheless, other possibilities such as HIF localization in the pre-mRNA splicing machinery (for a review, see [Lamond and Spector, 2003]) cannot be entirely excluded.

Along with the well-known interaction between C-TAD in HIF-1α and CH1 in p300, a recent study has discovered that N-TAD can interact with CH3 in CBP/p300, strongly supporting the role of N-TAD in transactivation [Ruas et al., 2010]. However, discriminating between two TADs eliciting transactivation is not a trivial issue because the stability of HIF-1α itself is directly connected to the N-TAD modification by PHD2. To elucidate the role of each TAD, an experimental method based on VHL deficient RCC4 cells for stable expression of HIF-1α has been introduced [Tian et al., 2011]. Employing hydroxyl residue-specific antibodies, three hydroxyl groups in HIF-1α (Pro402 and Pro564 in N-TAD, and Asn803 in C-TAD) were found to possess varying sensitivities to the oxygen level, demonstrating the feasibility of non-redundant roles of C-TAD and N-TAD transactivation as a function of oxygen concentrations. Although these antibodies permitted analyzing effects of different modes of hydroxylase inhibition on different sites of HIF-1α hydroxylation, the immune-detection method may not be appropriate for cell-based drug screening of hydroxylase inhibitors in large scale. In parallel, a gene silencing approach by siRNAs has enabled to identify which PHD is essential to stabilize HIF-1α [Berra et al., 2003], and to discriminate HIF target genes sensitive to FIH-1 expression and C-TAD transactivation [Dayan et al., 2006]. When employing siRNAs, it is important to confirm that silencing genes by siRNAs does not cause any nonspecific effects such as off-target effects and inhibition of endogenous mRNA function. With a simple transient transfection easily adoptable for small molecule screening, we demonstrated that FRET measurements could probe the direct interaction between C-TAD and CH1 in living cells. Consistent to the previous report [Tian et al., 2011], we found that DFO effects could not be simply explained by its inhibition on HIF-specific hydroxylases, implying that the inhibition mechanism might be more complex. Although the present study specifically focused on the interaction between C-TAD and CH1, it would be interesting to probe how each TAD activity changes as a function of oxygen concentrations or in the presence of various small molecules. As successfully used to monitor the activities of two different proteins in real time [Ouyang et al., 2010], applying two FRET pairs will provide more insights into the roles of two TADs in the HIF-mediated signaling pathway.

ACKNOWLEDGMENTS

This work was supported by the Proteogenomics Research Program funded by the Korean Ministry of Education, Science and Technology, and by the KIST grant.

REFERENCES

Appelhoff RJ, Tian YM, Raval RR, Turley H, Harris AL, Pugh CW, Ratcliffe PJ, Gleadle JM. 2004. Differential function of the prolyl hydroxylases PHD1, PHD2, and PHD3 in the regulation of hypoxia-inducible factor. J Biol Chem 279:38458–38465.

Berra E, Benizri E, Ginouves A, Volmat V, Roux D, Pouyssegur J. 2003. HIF prolyl-hydroxylase 2 is the key oxygen sensor setting low steady-state levels of HIF-1α in normoxia. EMBO J 22:4082–4090.

Brahimi-Horn MC, Pouyssegur J. 2007. Harnessing the hypoxia-inducible factor in cancer and ischemic disease. Biochem Pharmacol 73:450–457.

Carrero G, McDonald D, Crawford E, de Vries G, Hendzel MJ. 2003. Using FRAP and mathematical modeling to determine the in vivo kinetics of nuclear proteins. Methods 29:14–28.

Cereseto A, Manganaro L, Gutierrez MI, Terreni M, Fittipaldi A, Lusic M, Marcello A, Giacca M. 2005. Acetylation of HIV-1 integrase by p300 regulates viral integration. EMBO J 24:3070–3081.

Chan DA, Kawahara TL, Sutphin PD, Chang HY, Chi JT, Giaccia AJ. 2009. Tumor vasculature is regulated by PHD2-mediated angiogenesis and bone marrow-derived cell recruitment. Cancer Cell 15:527–538.

Chiang CF, Okou DT, Griffin TB, Verret CR, Williams MN. 2001. Green fluorescent protein rendered susceptible to proteolysis: Positions for protease-sensitive insertions. Arch Biochem Biophys 394:229–235.

Cho H, Park H, Yang EG. 2005. A fluorescence polarization-based interaction assay for hypoxia-inducible factor prolyl hydroxylases. Biochem Biophys Res Commun 337:275–280.

Choi SM, Choi KO, Park YK, Cho H, Yang EG, Park H. 2006. Clioquinol, a Cu(II)/Zn(II) chelator, inhibits both ubiquitination and asparagine hydroxylation of hypoxia-inducible factor-1α, leading to expression of vascular endothelial growth factor and erythropoietin in normoxic cells. J Biol Chem 281:34056–34063.

Cook KM, Hilton ST, Mecinovic J, Motherwell WB, Figg WD, Schofield CJ. 2009. Epidithiodiketopiperazines block the interaction between hypoxia-inducible factor-1α (HIF-1α) and p300 by a zinc ejection mechanism. J Biol Chem 284:26831–26838.

Dames SA, Martinez-Yamout M, De Guzman RN, Dyson HJ, Wright PE. 2002. Structural basis for Hif-1α/CBP recognition in the cellular hypoxic response. Proc Natl Acad Sci USA 99:5271–5276.

Dayan F, Roux D, Brahimi-Horn MC, Pouyssegur J, Mazure NM. 2006. The oxygen sensor factor-inhibiting hypoxia-inducible factor-1 controls expression of distinct genes through the bifunctional transcriptional character of hypoxia-inducible factor-1α. Cancer Res 66:3688–3698.

Dayan F, Monticelli M, Pouyssegur J, Pecou E. 2009. Gene regulation in response to graded hypoxia: The non-redundant roles of the oxygen sensors PHD and FIH in the HIF pathway. J Theor Biol 259:304–316.

Ema M, Hirota K, Mimura J, Abe H, Yodoi J, Sogawa K, Poellinger L, Fujii-Kuriyama Y. 1999. Molecular mechanisms of transcription activation by HLF and HIF1α in response to hypoxia: Their stabilization and redox signal-induced interaction with CBP/p300. EMBO J 18:1905–1914.

Freedman SJ, Sun ZY, Poy F, Kung AL, Livingston DM, Wagner G, Eck MJ. 2002. Structural basis for recruitment of CBP/p300 by hypoxia-inducible factor-1α. Proc Natl Acad Sci USA 99:5367–5372.

Girdwood D, Bumpass D, Vaughan OA, Thain A, Anderson LA, Snowden AW, Garcia-Wilson E, Perkins ND, Hay RT. 2003. p300 transcriptional repression is mediated by SUMO modification. Mol Cell 11:1043–1054.

Groulx I, Lee S. 2002. Oxygen-dependent ubiquitination and degradation of hypoxia-inducible factor requires nuclear-cytoplasmic trafficking of the von Hippel–Lindau tumor suppressor protein. Mol Cell Biol 22:5319–5336.

Gu J, Milligan J, Huang LE. 2001. Molecular mechanism of hypoxia-inducible factor 1α-p300 interaction. A leucine-rich interface regulated by a single cysteine. J Biol Chem 276:3550–3554.

Hachet-Haas M, Converset N, Marchal O, Matthes H, Gioria S, Galzi JL, Lecat S. 2006. FRET and colocalization analyzer-A method to validate measurements of sensitized emission FRET acquired by confocal microscopy and available as an ImageJ plug-in. Microsc Res Tech 69:941–956.

Hager GL, McNally JG, Misteli T. 2009. Transcription dynamics. Mol Cell 35:741–753.

Hirsila M, Koivunen P, Gunzler V, Kivirikko KI, Myllyharju J. 2003. Characterization of the human prolyl 4-hydroxylases that modify the hypoxia-inducible factor. J Biol Chem 278:30772–30780.

Hirsila M, Koivunen P, Xu L, Seeley T, Kivirikko KI, Myllyharju J. 2005. Effect of desferrioxamine and metals on the hydroxylases in the oxygen sensing pathway. FASEB J 19:1308–1310.

Huang LE, Gu J, Schau M, Bunn HF. 1998. Regulation of hypoxia-inducible factor 1α is mediated by an O_2-dependent degradation domain via the ubiquitin-proteasome pathway. Proc Natl Acad Sc. USA 95:7987–7992.

Kallio PJ, Okamoto K, O'Brien S, Carrero P, Makino Y, Tanaka H, Poellinger L. 1998. Signal transduction in hypoxic cells: Inducible nuclear translocation and recruitment of the CBP/p300 coactivator by the hypoxia-inducible factor-1α. EMBO J 17:6573–6586.

Kallio PJ, Wilson WJ, O'Brien S, Makino Y, Poellinger L. 1999. Regulation of the hypoxia-inducible transcription factor 1α by the ubiquitin-proteasome pathway. J Biol Chem 274:6519–6525.

Koivunen P, Hirsila M, Gunzler V, Kivirikko KI, Myllyharju J. 2004. Catalytic properties of the asparaginyl hydroxylase (FIH) in the oxygen sensing pathway are distinct from those of its prolyl 4-hydroxylases. J Biol Chem 279:9899–9904.

Kung AL, Zabludoff SD, France DS, Freedman SJ, Tanner EA, Vieira A, Cornell-Kennon S, Lee J, Wang B, Wang J, Memmert K, Naegeli HU, Petersen F, Eck MJ, Bair KW, Wood AW, Livingston DM. 2004. Small molecule blockade of transcriptional coactivation of the hypoxia-inducible factor pathway. Cancer Cell 6:33–43.

Lamond AI, Spector DL. 2003. Nuclear speckles: A model for nuclear organelles. Nat Rev Mol Cell Biol 4:605–612.

Lando D, Peet DJ, Gorman JJ, Whelan DA, Whitelaw ML, Bruick RK. 2002. FIH-1 is an asparaginyl hydroxylase enzyme that regulates the transcriptional activity of hypoxia-inducible factor. Genes Dev 16:1466–1471.

Maxwell PH, Wiesener MS, Chang GW, Clifford SC, Vaux EC, Cockman ME, Wykoff CC, Pugh CW, Maher ER, Ratcliffe PJ. 1999. The tumour suppressor protein VHL targets hypoxia-inducible factors for oxygen-dependent proteolysis. Nature 399:271–275.

Min JH, Yang H, Ivan M, Gertler F, Kaelin WG, Jr., Pavletich NP. 2002. Structure of an HIF-1 α-pVHL complex: Hydroxyproline recognition in signaling. Science 296:1886–1889.

Moroz E, Carlin S, Dyomina K, Burke S, Thaler HT, Blasberg R, Serganova I. 2009. Real-time imaging of HIF-1α stabilization and degradation. PLoS ONE 4:e5077.

Mueller F, Mazza D, Stasevich TJ, McNally JG. 2010. FRAP and kinetic modeling in the analysis of nuclear protein dynamics: What do we really know? Curr Opin Cell Biol 22:403–411.

Nardinocchi L, Pantisano V, Puca R, Porru M, Aiello A, Grasselli A, Leonetti C, Safran M, Rechavi G, Givol D, Farsetti A, D'Orazi G. 2010. Zinc downregulates HIF-1α and inhibits its activity in tumor cells in vitro and in vivo. PLoS ONE 5: e15048.

Ohh M, Park CW, Ivan M, Hoffman MA, Kim TY, Huang LE, Pavletich N, Chau V, Kaelin WG. 2000. Ubiquitination of hypoxia-inducible factor requires direct binding to the beta-domain of the von Hippel–Lindau protein. Nat Cell Biol 2:423–437.

Ouyang MX, Huang H, Shaner NC, Remacle AG, Shiryaev SA, Strongin AY, Tsien RY, Wang YX. 2010. Simultaneous visualization of protumorigenic Src and MT1-MMP activities with fluorescence resonance energy transfer. Cancer Res 70:2204–2212.

Patterson GH, Piston DW, Barisas BG. 2000. Forster distances between green fluorescent protein pairs. Anal Biochem 284:438–440.

Pelletier J, Dayan F, Durivault J, Ilc K, Pecou E, Pouyssegur J, Mazure NM. 2012. The asparaginyl hydroxylase factor-inhibiting HIF is essential for tumor growth through suppression of the p53-p21 axis. Oncogene 31:2989–3001.

Piston DW, Kremers GJ. 2007. Fluorescent protein FRET: The good, the bad and the ugly. Trends Biochem Sci 32:407–414.

Ruas JL, Poellinger L, Pereira T. 2002. Functional analysis of hypoxia-inducible factor-1α-mediated transactivation. Identification of amino acid residues critical for transcriptional activation and/or interaction with CREB-binding protein. J Biol Chem 277:38723–38730.

Ruas JL, Poellinger L, Pereira T. 2005. Role of CBP in regulating HIF-1-mediated activation of transcription. J Cell Sci 118:301–311.

Ruas JL, Berchner-Pfannschmidt U, Malik S, Gradin K, Fandrey J, Roeder RG, Pereira T, Poellinger L. 2010. Complex regulation of the transactivation function of hypoxia-inducible factor-1α by direct interaction with two distinct domains of the CREB-binding protein/p300. J Biol Chem 285:2601–2609.

Salceda S, Caro J. 1997. Hypoxia-inducible factor 1α (HIF-1α) protein is rapidly degraded by the ubiquitin-proteasome system under normoxic conditions. Its stabilization by hypoxia depends on redox-induced changes. J Biol Chem 272:22642–22647.

Semenza GL. 2003. Targeting HIF-1 for cancer therapy. Nat Rev Cancer 3:721–732.

Semenza GL. 2011. Mechanism of disease. Oxygen sensing, homeostasis, and disease. N Engl J Med 365:537–547.

Tian YM, Yeoh KK, Lee MK, Eriksson T, Kessler BM, Kramer HB, Edelmann MJ, Willam C, Pugh CW, Schofield CJ, Ratcliffe PJ. 2011. Differential sensitivity of hypoxia inducible factor hydroxylation sites to hypoxia and hydroxylase inhibitors. J Biol Chem 286:13041–13051.

Wenger RH. 2002. Cellular adaptation to hypoxia: O_2-sensing protein hydroxylases, hypoxia-inducible transcription factors, and O_2-regulated gene expression. FASEB J 16:1151–1162.

Wotzlaw C, Otto T, Berchner-Pfannschmidt U, Metzen E, Acker H, Fandrey J. 2007. Optical analysis of the HIF-1 complex in living cells by FRET and FRAP. FASEB J 21:700–707.

Wotzlaw C, Gneuss S, Konietzny R, Fandrey J. 2010. Nanoscopy of the cellular response to hypoxia by means of fluorescence resonance energy transfer (FRET) and new FRET software. PMC Biophys 3:5.

Xie Z, Zhang ZL, Zou X, Huang J, Ruas P, Thompson D, Shen QJ. 2005. Annotations and functional analyses of the rice WRKY gene superfamily reveal positive and negative regulators of abscisic acid signaling in aleurone cells. Plant Physiol 137:176–189.

SUPPORTING INFORMATION

Additional supporting information may be found in the online version of this article at the publisher's web-site.